Seasonal cycle and long-term trend of solar energy fluxes through Arctic sea ice

Stefanie Arndt [1]*, Marcel Nicolaus [1]

[1] Alfred-Wegener-Institut Helmholtz-Zentrum für Polar- und Meeresforschung, Bremerhaven, Bussestraße 24, 27570 Bremerhaven, Germany

* Correspondence to:
Stefanie Arndt
Alfred-Wegener-Institut Helmholtz-Zentrum für Polar- und Meeresforschung
Bussestraße 24
27570 Bremerhaven
Germany

E-Mail: stefanie.arndt@awi.de
Phone: +49 471 4831 2140
Fax: +49 471 4831 1797

Abstract

Arctic sea ice has not only decreased in volume during the last decades, but has also changed in its physical properties towards a thinner and more seasonal ice cover. These changes strongly impact the energy budget and might affect the ice-associated ecosystems. In this study we quantify solar shortwave fluxes through sea ice for the entire Arctic during all seasons. To focus on sea ice related processes, we exclude fluxes through open water, scaling linearly with sea ice concentration. We present a new parameterization of light transmittance through sea ice for all seasons as a function of variable sea ice properties. The maximum monthly mean solar heat flux under the ice of 30×10^5 Jm^{-2} occurs in June, enough heat to melt 0.3 m of sea ice. Furthermore, our results suggest that 96% of the annual solar heat input through sea ice occurs during only a four month period from May to August. Applying the new parameterization on remote sensing and reanalysis data from 1979 to 2011, we find an increase in transmitted light of 1.5%/year for all regions. This corresponds to an increase in potential sea ice bottom melt of 63% over the 33 year study period. Sensitivity studies reveal that the results strongly depend on the timing of melt onset and the correct classification of ice types. Assuming two weeks earlier melt onset, the annual transmitted solar radiation to the upper ocean increases by 20%. Continuing the observed transition from a mixed multi-year/first-year sea ice cover to a seasonal ice cover results in an increase of light transmittance by an additional 18 %.

1. Introduction

The evolution of Arctic sea ice towards a thinner, younger, and more seasonal sea ice cover during the last few decades (e.g. Comiso, 2012;Haas et al., 2008;Maslanik et al., 2011;Maslanik et al., 2007) has a strong impact on the partitioning of solar energy between the atmosphere, sea ice, and ocean (e.g. 2011a;Perovich et al., 2007b;Wang et al., 2014). Decreased surface albedo (Perovich et al., 2011a), earlier melt onset, and a longer melt season (Markus et al., 2009, updated) have contributed to the observed increases in sea ice and snow melt (Perovich and Richter-Menge, 2009), and higher absorption and transmission of solar irradiance within and through Arctic sea ice (Nicolaus et al., 2012;Stroeve et al., 2014). Beyond the physical consequences of the observed changes, strong impacts on ecological interactions and biogeochemical processes are expected, such as changes in habitat conditions for ice-associated organisms or changes in primary production (Arrigo et al., 2012;Deal et al., 2011;Popova et al., 2012).

Various studies have shown the immediate link between sea ice energy and mass balance, as well as the impact of energy fluxes on the physical properties of sea ice (Grenfell et al., 2006;Light et al., 2008;Perovich and Richter-Menge, 2009). These heat fluxes are composed of short-wave, long-wave, conductive, and turbulent fluxes at the interfaces of sea ice with the atmosphere and the ocean. Beyond these energy budget approaches, sea ice mass balance may also be derived from direct comparisons of sea ice growth during winter, and surface and bottom melt during summer (Perovich et al., 2011b).

From studies on the interaction of sunlight and sea ice, it has been possible to improve our understanding of the effects of snow cover (Perovich et al., 2007b), melt ponds (Rösel and Kaleschke, 2012;Schröder et al., 2014), and biological interactions (Arrigo et

al., 2012;Mundy et al., 2005;2007). In addition, the spatial variability (Perovich et al., 2011a) and seasonal changes (Nicolaus et al., 2010a;Perovich et al., 2002;Perovich and Polashenski, 2012) in the optical properties of sea ice and snow have been studied by different methods. However, previous studies have not quantified large-scale, multi-seasonal, and inter-annual changes, because these studies were limited to different regions and/or seasons of the year. In addition, these studies have described measurements on different ice types, which also differ in their optical properties as a result of their growth history (Perovich and Polashenski, 2012). One possible approach to obtain such generalized studies on the in- and under-ice energy budgets in sea-ice covered oceans would be to use a radiative transfer model in combination with surface energy budgets, as implemented by Perovich et al. (2011a). However, such a model would require adequate knowledge about the distribution of snow and sea ice (as forcing data) to derive the optical properties of sea ice and snow as a function of space and time. This type of information is not available yet, in particular not for time scales on the order of decades. An alternative approach is to use existing remote sensing and re-analyses data together with a parameterization of light transmittance through sea ice. This method was developed by Nicolaus et al. (2012) and (2013) to calculate Arctic-wide radiation fluxes through sea ice. However, these studies were restricted to one month (August 2011), when comprehensive in-situ measurements are available from the trans-polar cruise of the German research vessel Polarstern.

In order to improve the understanding of the ongoing change in sea ice conditions and the associated impact on the partitioning of solar energy, we provide an estimate of the monthly shortwave radiative transfer through sea ice for the entire Arctic Ocean for the period 1979 to 2011. To emphasize the changing physical properties of the Artic sea ice

cover, our estimates include fluxes through sea ice only. Therefore, we use a definition of 6 types of sea ice over the annual cycle, define 6 distinct time periods of insolation conditions, and include the temporal and spatial variability of melt ponds to extend and generalize the up-scaling method of Nicolaus et al. (2012) and (2013). In order to investigate the reliability of the method and to obtain a measure of uncertainty, we perform sensitivity studies by comparing the calculated fluxes to in-situ observations obtained from the Transpolar Drift, between 86.5° and 88.5°N, during the drift study of the schooner Tara from April to September 2007 (Nicolaus et al., 2010a). Finally, it was possible to estimate transmitted heat fluxes through sea ice and derive trends for the entire Arctic basin for the period of 1979 to 2011. Since this study focuses on the variability of sea ice properties, changes in sea ice concentration are not considered.

2. Methods

Solar short-wave radiation fluxes (250 to 2500 nm, here also referred to as "light") through sea ice are calculated daily, from 01 January 1979 to 31 December 2011, for the entire Arctic Ocean (north of 65°N). Building on the method and parameterization by Nicolaus et al. (2012) and (2013), which was limited to the snow-free summer season in 2011 without any seasonal cycle of surface properties, the parameterization of light transmittance through sea ice has been extended for all seasons. Thus, transmittance is now estimated as a function of surface (snow) melt/freeze state and melt pond concentration, in addition to the previous (only) sea ice age dependence. The new parameterization was driven by satellite observations of daily sea ice concentration and surface solar irradiance to calculate fluxes as performed in Nicolaus et al. (2012) and (2013). All data sets are interpolated to a 10-km polar stereographic grid, using nearest

neighbor resampling. Although daily fluxes are calculated and available, only monthly means are shown and used to discuss the findings, because the main focus of this extended study is on seasonal changes and long-term trends.

For the main analyses we exclude open water areas as those would clearly dominate the transmitted heat flux signal (Perovich et al., 2007a). Therefore, we consider only fluxes through ice-covered areas as these are crucial for the energy and mass balance of sea ice as well as for biological processes beneath the ice cover. The solar heat input to the open ocean has also an important impact on the ice-ocean system but is a basic function of sea ice concentration.

2.1 Solar heat flux equations

Solar heat input through sea ice into the ocean ($E_T(t,x,y)$) is calculated as the product of the downward solar radiation (E_d), the sea ice concentration (C_i), and the total transmittance of pond covered sea ice (τ_i) for each grid cell and each day, over the period 01 January 1979 to 31 December 1999:

$$E_T(t,x,y) = E_d(t,x,y) \cdot C_i(t,x,y) \cdot \tau_i \qquad \textbf{(1)}$$

with time (t) and position (x,y).

Since 01 January 2000, when satellite derived melt-pond concentrations are available, the solar heat input through sea ice into the ocean (E_T) is calculated as the sum of fluxes through bare ice (E_B) and melt ponds (E_P):

$$E_T(t,x,y) = E_B(t,x,y) + E_P(t,x,y)$$

$$E_T(t,x,y) = E_d(t,x,y) \cdot C_i(t,x,y) \cdot \left[1 - C_p(t,x,y)\right] \cdot \tau_b(t,x,y) + E_d(t,x,y) \cdot C_i(t,x,y) \cdot C_p(t,x,y) \cdot \tau_p(t,x,y) \qquad \textbf{(2)}$$

with the transmitted solar radiation at the bottom of the ice E_T, downward solar radiation E_d, sea ice concentration C_i, melt pond fraction C_p, transmittance of bare sea ice τ_b, transmittance of melt ponds τ_p, time t and grid cell (x,y).

To obtain the total solar heat input per unit area for a certain time period ($Q_T(x,y)$), the heat flux is calculated for each grid cell and then integrated over the given time (Δt)

$$Q_T(x, y) = \sum E_T(t, x, y)\, \Delta t. \qquad \textbf{(3)}$$

Spatial integration over the entire Arctic Ocean (north of 65°N), reveals the Arctic-wide total solar heat input Q_T.

Assuming sea ice is at its melting point, has a density ρ_{ice} of 917 kg m^{-3} and has a latent heat of fusion L_{ice} of 0.3335 J kg^{-1}; and there are no changes in longwave, latent, and conductive heat fluxes, $Q_T(x,y)$ can be converted into a sea ice melt rate m_{eq}:

$$m_{eq} = \frac{Q_T(x,y)}{L_{melt} \cdot \rho_{ice}}. \qquad \textbf{(4)}$$

2.2 Seasonality of surface properties and transmittance of Arctic sea ice

To calculate solar heat fluxes under Arctic sea ice for an entire year, the main challenge is to parameterize the seasonal evolution of $\tau_b(t,x,y)$. This is mainly achieved by merging the sea-ice age information (Maslanik et al., 2007;2011) with the melt/freeze status (Markus et al., 2009, updated) into six surface types.

2.2.1 Definition of sea ice types

Figure 1 shows the annual cycle of these six sea ice classes together with surface properties of Arctic sea ice. These classes are introduced to avoid abrupt changes in the

optical properties during the transition from spring to summer as well as from summer to fall. After early melt onset (EMO), *melting FYI* and *melting MYI* are introduced for sea ice completely melting during the summer melt. Therefore, it is necessary to classify each cell as either becoming ice free (sea ice concentration less than 15%) or not. To do this, the ice concentration of each pixel is evaluated for all days until EFO. If the pixel becomes ice free, the last day of melting is stored for later calculations. According to Maslanik et al. (2007) and (2011), *FYI* surviving the summer melt turns into *MYI* after week 36 of the year. As the immediate change in ice age tagging is not associated with an immediate change in sea ice properties, we include an additional class of *new MYI* that turns into *MYI* at the end of the year. When sea ice concentration reaches a value greater than 15% the pixel is classified as *new FYI*.

In the following, sea ice consisting of both bare sea ice and melt ponds is called pond covered sea ice.

2.2.2 Transmittance of pond covered sea ice

The seasonal evolution of surface properties and transmittance of Arctic sea ice is divided into six different phases (note that there are both different ice types and different seasonal phases). The timing of these phases is based on the melt and freeze onset data established by Markus et al. (2009, updated). Our parameterization of seasonal variations in light transmittance considers the transmission through both sea ice and snow and is mostly based on the results of two field campaigns that focused on the understanding of ice-ocean-atmosphere processes that control the partitioning of solar radiation among reflection, absorption, and transmittance: The Surface Heat Budget of the Arctic Ocean experiment (SHEBA) from 1997 to 1998 (Perovich, 2005); and measurements conducted on MYI within the Transpolar Drift, between 86.5° and

88.5°N, during the drift study of the schooner Tara from April to September 2007 (Nicolaus et al., 2010a). In addition, analyses from previous observations by Perovich (1996), Perovich et al. (1998), and Nicolaus et al. (2010b) are used. Figure 2a shows the seasonal total transmittance of pond covered sea ice (τ_i) for constant pond concentrations of 26 (FYI) and 29 % (MYI), respectively, used for the period 1979 to 2000, during which time there are no available satellite melt pond coverage observations. This combination of a given mixture of ponds and bare ice was used to develop the seasonal cycle of transmittance, as described in the next paragraphs. All transmittance values for the different phases are compiled in Table 2.

Phase I: Winter (from FO+60 days to EMO)

Winter conditions are characterized by snow covered sea ice without melt ponds. The snow cover is assumed to be cold, dry and optically thick, which means the snow determines the optical properties. Thus, radiative fluxes through sea ice are small. The best available transmittance observations for such conditions are those measured during the first days of the Tara drift, although it was already early April. Hence transmittance was accordingly set to 0.002 (Nicolaus et al., 2010a).

Phase II: Early melt (from EMO to MO)

EMO denotes the first significant change in optical properties. Snow depth decreases, and surface and sea ice temperatures increase. Consequently, the snow becomes wet and is no longer optically thick. This phase also corresponds to formation of the first melt ponds.. Here we assume a linear increase of τ_i until MO.

Nicolaus et al. (2010a) calculated a transmittance of 0.02 for MYI for the day of MO. Furthermore, Perovich and Polashenski (2012) reveal that the surface albedo of FYI is

about half that of MYI at the same time. Adapting this albedo evolution to the transmittance, the transmittance of FYI is assumed to be 0.04 at MO.

Melting FYI and melting MYI

After EMO, the continued melt of snow and sea ice strongly impacts light transmittance. Starting with the summer phase (phase IV), we assume that the optical properties of melting sea ice differ from sea ice surviving the summer melt. In addition, differences between melting FYI and melting MYI are expected. Therefore, melting FYI and melting MYI are separated in the parameterization of τ_i.

In order to describe these classes, laboratory studies by Perovich (1996) on the evolution of albedo during the initial ice growth phase were applied to the evolution of transmittance assuming an inverse behavior of transmittance and albedo. Therefore, the increase in transmittance of seasonal sea ice can be described as roughly exponential (Perovich, 1996). Assuming the transition of transmittance from melting sea ice to open ocean is inverse of the albedo transition (Perovich, 1996), we use a transmittance of 0.4 for the last remaining sea ice. Thus, an exponential increase between the first and last day of melting for the according pixel is fitted and the maximum transmittance of sea ice is expected to be 0.4.

Phase III: Continuous melt (from MO to MO+14 days)

After MO, snow is assumed to melt completely within 14 days (Nicolaus et al., 2006;Perovich et al., 2002) and pond cover fraction increases rapidly until the maximum pond cover is reached at the end of this phase (Nicolaus et al., 2010a). The transmittance continues to increase linearly until the beginning of summer (MO+14 days).

246 *Phase IV: Summer (from MO+14 days to EFO)*

247 During this phase the sea ice surface is characterized by strong sea ice melt and
248 culminates in the minimum ice concentration of each pixel. The surface is a mixture of
249 bare ice and melt ponds with a constantly renewing surface scattering layer (Perovich et
250 al., 2002;Barber et al., 1998). This implies small changes of optical properties and light
251 transmittance of the ice over time during Phase IV. Hence, τ_i is assumed to be constant
252 for sea ice that survives summer melt. Based on observed transmittance values of solar
253 radiation through FYI and MYI during TransArc 2011 (Nicolaus et al., 2012), we use
254 summer transmittance values of 0.04 for bare FYI, 0.01 for bare MYI, 0.22 for melt ponds
255 on FYI, and 0.15 for melt ponds on MYI. These values are weighted according to melt
256 pond fractions (Rösel and Kaleschke, 2012).

257

258 *Phase V: Fall freeze-up (from EFO to FO)*

259 Air and surface temperatures drop below 0°C resulting in the initial occurrence of
260 surface freezing. Subsequently, snow accumulation can begin and former melt ponds
261 refreeze but can still be recognized through the new snow cover. Thus, the
262 transmittance is decreasing rapidly. Similar to Phase III the transmittance of FYI
263 decreases to 0.04 and for MYI to 0.02 until FO. Additionally, sea ice that survives the
264 summer melt is promoted to one-year-older ice in week 36/37 according to Maslanik et
265 al. (2007) and new ice forms. The transmittance of new first year ice evolves
266 correspondingly to the melting sea ice surface, described above. From EFO until the
267 beginning of winter (FO+60 days), the strong growth of sea ice (e.g., increasing sea ice
268 thickness) results in an exponential decrease in light transmission through newly
269 formed FYI.

270

Phase VI: Continuous freeze (from FO to FO+60 days)

This phase is characterized by continuous freezing, increasing snow accumulation towards an optically thick snow layer, and the gradual disappearance of melt ponds. In addition to new sea ice formation, the existing sea ice is getting thicker, older, and deformation is increasing. Transmittance decreases back to 0.02 by winter. It is assumed that at the end of the freezing phase (FO+60 days) the surface properties of all newly formed FYI can be considered as equivalent. Afterwards, the accumulated optically thick snow layer again dominates the optical properties of FYI and MYI (Phase I).

2.2.3 Transmittance of bare ice and ponds

For the period after the year 2000, when satellite derived melt pond products are available from Rösel and Kaleschke (2012), the transmittance values of bare ice (τ_b) and ponds (τ_p) are treated separately (Figure 2b). The modal transmittance of melt ponds is constant over the entire melt season. It is set to 0.22 for FYI and 0.15 for MYI, as measured during TransArc 2011 (Nicolaus et al., 2012). The seasonal evolution of transmittance for bare ice (τ_b) follows the transmittance for pond covered sea ice (τ_i):

$$\tau_b(x,y) = \tau_i(x,y) \cdot \frac{\tau_b(summer,x,y)}{\tau_i(summer,x,y)} \quad \textbf{(4)}$$

The values of τ_b(summer,x,y) and τ_i(summer,x,y) are the constant values during summer as given in Table 2. Thus, the ratio of both is constant for MYI (0.20) and FYI (0.46). Finally, those transmittance values are scaled with the pond concentrations, as given in Equation 2.

2.3 Deriving trends

Based on the calculated results of the solar heat input through sea ice into the ocean, trends are analyzed for the period 1979 to 2011. The trends (monthly and annual) are

calculated by a linear least-squares fit of the total mean (monthly or annual) heat flux for each grid cell ($Q_T(x,y)$). Resulting trends are normalized by trends in sea ice concentration, because here we focus on radiative fluxes through the ice-covered part of the ocean. Otherwise the results would strongly depend on regional and temporal trends in sea ice concentration, because of the high transmittance (0.93) of open water. All trends were calculated for both the annual mean ice covered area in 2011 and the monthly mean ice covered area in 2011 (sea ice concentration > 15%) to allow for a representative comparison. Regions that were not ice covered at any time in 2011 are excluded from the main analysis and discussion.

2.4 Input data sets

The following satellite and re-analyses data sets were used (Tab. 1):

(1) Sea ice concentration observations were obtained from the Special Sensor Microwave Imager (SSMI/S) provided through the Ocean and Sea Ice Satellite Application Facilities (OSI SAF, product ID: OSI-401, Andersen et al. (2007)). For this study, a combination of reprocessed data (1979 to 2007) and operational data (2008 to 2011) was used. Both data sets have systematic differences due to processing with a different set of tie point statistics for the ice concentration algorithm (Lavergne et al., 2010). However, within the documented uncertainties both data sets build the best available and consistent time series of sea ice concentration. There is no consistent uncertainty for the data product but different approaches for determining uncertainties are described in Lavergne et al. (2010).

(2) For sea ice age, we used the updated data product by Maslanik et al. (2007) and (2011). This product is available since 1979 and is based on satellite derived ice motion data calculated from different sensors using a Lagrangian feature tracking algorithm.

Although this data product distinguishes ice ages between 1 to 10 years, here we only distinguish FYI and MYI (2 years and older), because all MYI is assumed to have similar optical properties. All data points with a sea ice concentration >0 but without an assigned sea ice age class were treated as FYI. Vice versa, all data points with sea ice concentration <15% but had an assigned sea ice age class were treated as open water. Such modifications were necessary to obtain consistent data products from the different sources, indicating partially varying sea ice extents. The ice age data set represents a 7-day average of either FYI or MYI without any uncertainty estimates. However, uncertainties in sea ice concentration and drift will have an impact on the ice age data.

(3) Downward surface solar radiation data were obtained four times per day from the European Centre for Medium-Range Weather Forecast (ECMWF) Era Interim re-analyses (Dee et al., 2011;Lindsay et al., 2014). The data (four values per day) were averaged to daily means and are available since 1979. Uncertainties for the data set are not reported.

(4) Sea ice surface characteristics were categorized by melt and freeze onset dates from passive microwave data (1979 to 2012) (Markus et al., 2009, updated). The data set distinguishes between the first occurrence of a melt event (early melt onset, EMO), the following continuous melt (melt onset, MO), the first occurrence of freeze-up conditions (early freeze onset, EFO), and the day of persistent freezing conditions (freeze onset, FO). The standard deviations, assumed as uncertainties, for the given dates are reported as EMO ± 3.6 days, MO ± 3.7 days, EFO ± 4.5 days, and FO ± 4.0 days (Markus et al., 2009, updated).

(5) Melt pond fraction was used from Rösel et al. (2012), retrieved from the Moderate Resolution Imaging Spectroradiometer (MODIS) onboard NASA's Terra and Aqua satellites. As this data set is only available since 2000, melt pond fractions from 1979 to

1999 were set to constant summer mean values of 26% for FYI and 29% for MYI as given in Rösel et al. (2012) for August 2011. In order to maintain consistency of the surface characteristics, all melt pond fractions before EMO are set to zero. The mean standard deviation from 2000 to 2011, assumed as uncertainty, is calculated as ± 3% for FYI and MYI.

We do not include snow depth and sea ice thickness as input data sets due to the lack of consistent high temporal resolution and long-term data products. Limitations of using sea ice age as an indirect proxy for ice thickness and snow cover as well as potential other approaches for the estimation of transmitted heat fluxes are discussed below.

3. Results

3.1 Seasonal cycle of solar radiation under Arctic sea ice in 2011

Based on the availability of all input data sets and the seasonality of transmittance values, the solar heat input through sea ice into the ocean is analyzed from 1979 to 2011. Figure 3 shows monthly mean heat input ($Q_T(x,y)$, Equation 3) under Arctic sea ice (ice covered areas only) from April to September 2011. The exemplary year 2011 was selected to ensure a representative comparison with previous studies conducted in August 2011 by Nicolaus et al. (2012) and (2013). From October to March the monthly mean solar radiation under sea ice was smaller than 0.2×10^5 Jm^{-2} with an Arctic-wide total under-ice heat flux (Q_T) of up to 0.4×10^{19} J. Since this represents less than 1% of the annual Arctic-wide heat flux of 53.3×10^{19} J (Equation 3), the months October to March are neglected from further analyses and discussion. In April the mean heat flux increased to 0.4×10^5 Jm^{-2} with a maximum of 7 to 8×10^5 Jm^{-2}, this amount of energy is equivalent to mean ice melt rates between 7 to 8 cm per month (Equation 4) in the

371 marginal ice zone East of Spitsbergen. The transmittance triples from 0.005 in April to
372 0.015 in May, and together with increasing surface fluxes, the $Q_T(x,y)$ increased from
373 1.0×10^{19} J to 5.5×10^{19} J during this time. The Barents Sea showed a mean transmitted
374 heat flux of 2.2×10^{5} Jm^{-2} for the month of May, with a maximum value of 25×10^{5} Jm^{-2},
375 which corresponds to a maximum sea ice melt of 25 cm per month. May to June showed
376 the most pronounced monthly increases in $Q_T(x,y)$ of 9.3×10^{5} Jm^{-2} and transmittance of
377 0.054 for the entire Arctic. The maximum $Q_T(x,y)$ was 30×10^{5} Jm^{-2} in June, with a
378 corresponding maximum melt rate of approximately 30 cm per month. June had also the
379 highest Q_T (20.9×10^{19} J), which was associated with the highest surface solar irradiance
380 over the entire Arctic Ocean (851×10^{19} J). This increase in solar irradiance was linked to
381 the beginning of the melt phase (mean MO on 30 May 2011) and associated rapid snow
382 melt. During this time, the difference between thin melting sea ice along the sea ice edge
383 and the persistent sea ice cover became most obvious, e.g. in the Chuckchi and Beaufort
384 Seas. In July, Arctic-wide averaged $Q_T(x,y)$ reached its annual maximum of 9.8×10^{5} Jm^{-2}.
385 This resulted primarily from the annual maximum in mean transmittance of 0.089, and
386 lead to a monthly flux Q_T of 18.4×10^{19} J. The impact of the different optical properties
387 (τ_i) of MYI and FYI became most obvious in July, because the difference of both values is
388 at its maximum. In addition, the strong decrease of sea ice concentration along the ice
389 edge became more important for the under-ice heat fluxes, because light transmittance
390 increased strongly in these regions. The August decrease of $Q_T(x,y)$ by more than 50% to
391 4.4×10^{5} Jm^{-2} along with only a slight reduction of transmittance to 0.084 can be
392 explained by the strong decrease in surface solar irradiance (679×10^{19} J). These surface
393 fluxes are only half of those calculated for previous months. August maximum $Q_T(x,y)$
394 reached up to 19×10^{5} Jm^{-2}. In September the $Q_T(x,y)$ decreased further to 0.6×10^{5} Jm^{-2},
395 which can be related to a low transmittance of 0.039 and Q_T of 0.7×10^{19} J.

3.2 Light transmission from 1979 to 2011

The new data set of $Q_T(x,y)$ allows quantification of annual budgets, regional differences, and decadal trends. Figure 4a shows the averaged annual solar heat input through sea ice into the ocean ($Q_T(x,y)$), and illustrates therefore the strong regional variability of $Q_T(x,y)$ ranging from 20 to 100 MJm^{-2} for the given period. This range in heat fluxes is equivalent to an ice melt rate of 24 to 120 cm per year. The mean total solar heat input transmitted through the considered sea ice covered area (section 2.3) was 46 MJm^{-2}.The maximum $Q_T(x,y)$ occurs at the edge of the marginal ice zone in the Canadian Arctic Archipelago (up to 110 MJm^{-2}/130 cm melt per year), and the East Siberian and Chukchi Seas (up to 80 MJm^{-2}/94 cm melt per year). In contrast, excluding areas characterized by a strong spring sea ice retreat and a corresponding low sea ice concentration, the minimum $Q_T(x,y)$ was found in the Central Arctic, a MYI dominated region of low transmittance.

The mean trend of $Q_T(x,y)$ was 1.5 $\%a^{-1}$ (excluding areas with a strong spring sea ice retreat) with a maximum of +4 $\%a^{-1}$ in the East Siberian Sea, and southern part of the North American and Russian Arctic Basin (Figures 4b and 5a). This trend translates to a 63% increase in the potential sea ice melt over the 33 year observation period. This is likely due to the prolongation of the melt season in the same regions. According to a linear regression from 1979 to 2011 for the entire Arctic, the mean MO was 4 days earlier, shifting from day 145 (24 May) to day 141 (20 May). The strongest trend of 4.8×10^{18} $J\,a^{-1}$ was found for June followed by May and July with 1.8×10^{18} $J\,a^{-1}$. August shows a comparably weak negative trend of -0.2×10^{18} $J\,a^{-1}$. Assuming an identical sea ice extent in 1979 and 2011, the increase in the annual mean solar heat flux through sea ice

(Q_T) amounts to 22.5×10^{19} J for the entire Arctic over the full study period. This corresponds to an average increase of 33%. Overall, 94% of the total annual solar heat input through Arctic sea ice was observed during the four key months: May to August. Furthermore, heat flux time series (annual, June, July) show an increasing variability after 1999 (Fig. 5).

4. Discussion

4.1 Seasonality and trends of transmitted fluxes

The total annual solar radiation under Arctic sea ice was estimated to be 53.3×10^{19} J in 2011. Based on this, May to August are the most important months for the radiative energy partitioning. During this period, 96% (51.2×10^{19} J) of the total annual solar heat input is transmitted through the sea ice. Extending the period to April to September, amounts to 99% (52.9×10^{19} J) of the total annual flux being transmitted within only a 6 month period. Generalizing the monthly fluxes, the annual cycle can be summarized into three phases: (1) The heat input through snow and sea ice into the ocean is negligible between October and March, (2) surface solar radiation dominates the under-ice light conditions from April to June, because transmittance increases only slowly, while surface irradiance determines most of the observed changes and variability, (3) during summer (July to September), energy fluxes depend mainly on the sea ice type, showing large differences in transmittance between FYI and MYI.

Comparing our results to the development of the solar heat input into the ice presented by Perovich et al. (2011a, Fig. 2), both the solar heat input to the upper ocean and the solar heat input to the sea ice demonstrated a positive annual trend of 1 to 1.5% per year during the last decades. The increasing energy in the ice and upper ocean might

446 both lead to a stronger sea ice melt. Therefore, the radiative heating of the upper ocean
447 might contribute to a higher conductive ocean heat flux to the ice. This increase in
448 bottom melt is affecting the sea ice mass balance. An increasing light absorption of Arctic
449 sea ice due to more seasonal ice and less multi-year ice was also found by Nicolaus et al.
450 (2012).
451
452 The trend towards more light transmission through sea ice, does not only impact the
453 light conditions right at the bottom of the sea ice, but also affects the horizontal and
454 vertical light field in the ice covered ocean. More light at the bottom of sea ice will
455 deepen the euphotic zone, as more light penetrates deeper into the ocean (Frey et al.,
456 2011;Katlein et al., 2014). More light can contribute to an increase in mixed layer
457 temperature, and provide more energy for primary production and biogeochemical
458 processes in and beneath the sea ice. However, it has to be noted that an increase in light
459 availability does not necessarily increase biological activity, but might also be harmful
460 (Leu et al., 2010).
461 An increase in transmittance will accelerate internal and bottom melt, which in turn will
462 reduce the thickness of sea ice and increase transmittance. That feedback process can
463 trigger a transmittance-melt feedback.
464
465 All presented trends are normalized with the trend in sea ice concentration (Section
466 2.3). Thus, changes related to physical properties of the sea ice are highlighted instead of
467 changes related to a general sea ice retreat. Fluxes through the ice-covered ocean will be
468 of great importance and are much more difficult to assess than fluxes through open
469 water. However, including the trend in sea ice concentration, the annual trend of
470 transmitted solar heat fluxes to the upper ocean decreases from +1.5% a^{-1} to ±1.1% a^{-1}.

471 The negative trend in the open ocean heat input is evident in areas of ice motion causing
472 an increase in ice concentration, which was also shown in Perovich et al. (2007a,2011a).
473 This comparison emphasizes the dominance of the albedo feedback mechanism and the
474 strong influence of the trend in sea ice concentration on the heat budget of the entire
475 system.
476 Beyond this, it is also important to consider that the trends in sea ice concentration
477 differ significantly during different months. While it is largest (-0.1% a^{-1}) in September,
478 it is only -0.06% a^{-1} in June, and even positive in April and May (+0.04% a^{-1}). This means
479 that the effect of increasing transmission through open water is particularly strong in
480 September, but less pronounced in June when highest absolute fluxes are observed, or in
481 spring when the impact on biological primary production is expected to be strongest
482 (Wassmann and Reigstad, 2011).
483
484 **4.2 Comparison with field data**
485 Validation of the calculated trends and spatial variability is nearly impossible as
486 insufficient field data with adequate spatial and temporal coverage are available.
487 However, some comparisons with time series of light transmission from different field
488 studies may be performed to identify major uncertainties.
489 Here we compare surface and transmitted solar irradiance of the presented method
490 with in-situ measurements during the Transpolar Drift of Tara from 29 April to 28
491 August 2007 (Nicolaus et al., 2010a). Nearest-neighbor grid points within 0.5° of the
492 daily Tara position were extracted from the presented data set and averaged. Figure 6a
493 (red and green lines) shows a comparison of the time series for transmitted solar
494 irradiance from both data sets. Until 08 June, the transmitted solar irradiance under sea
495 ice varied only slightly, around 0.5 Wm^{-2}, for both the calculated and the measured time

496 series. Afterwards, until the end of June, the measured transmitted fluxes increased
497 steadily towards 10 Wm^{-2}, whereas calculated fluxes were highly variable with most
498 values below 4 Wm^{-2}. Hence, the total solar heat input through the sea ice to the ocean
499 from 1 May to 16 July 2007 was 21.4 MJm^{-2} for the observed Tara data, whereas the
500 calculated data resulted in a 17% lower total heat flux of 17.7 MJm^{-2}. The calculated
501 underestimation is equivalent to 1 cm of sea ice melt for this period. During summer (16
502 July to 14 August 2007), under-ice fluxes cannot be reliably compared since the sensor
503 at the Tara study was strongly influenced by biological processes in ice and water,
504 causing an increased absorption and reduced transmitted fluxes. Thus, the calculated
505 fluxes were overestimated by 11.6 MJm^{-2}, representing an equivalent sea ice melt of 4
506 cm during summer.
507 After 14 August, the measured transmitted heat flux increased rapidly to about 6 Wm^{-2},
508 comparable to the calculated value. Finally, the decrease in solar elevation caused
509 decreasing transmitted fluxes in both data sets, resulting in similar heat fluxes of
510 0.28×10^3 MJm^{-2} after 14 August.
511 The main reason for these differences is the timing of the phases describing the surface
512 characteristics. While both data sets have a coincident EMO on 09 June, large differences
513 are evident for the later phase transitions: The observed MO at Tara was on 21 June
514 whereas the calculated MO for the center position was 17 days later on 8 July.
515 Considering the 8 neighboring cells results in a mean MO on 13 June. This shows that
516 there is a difference of 25 days in MO for the 10 km grid. As presented above, the
517 transmitted heat flux strongly depends on the timing of the different melt phases by
518 Markus et al. (2009). EFO was observed on 15 August during Tara, whereas the satellite
519 data maintains summer melt conditions until 14 September. However, the total solar
520 heat input through sea ice was similar for both data sets. Thus, the solar radiation flux

under Arctic sea ice strongly depends on the timing of EMO and MO, while the timing of EFO and FO seems to be of less importance since the beginning of the melt season coincides with maximum surface solar heat fluxes. The timing of melt onset also has a large influence on the total amount of light absorption, as shown in Stroeve et al. (2014). Including the ongoing lengthening of the melt season by up to two weeks per decade (by a later EMO), Stroeve et al. (2014)'s calculations suggest an albedo decrease of 9% per decade.

In a second validation step, the heat fluxes were re-calculated using the onset dates as observed during Tara instead of those by Markus et al. (2009) (Figure 6, black lines). This eliminated the impact of the onset dates on the results. Nevertheless, the calculated total solar heat input through sea ice was still differing by 18% (25.4 MJm^{-2}) from the Tara fluxes until 16 July (Figure 6a) due to an unexpected peak in $Q_T(x,y)$ in July. In addition, the calculated time series still showed large day-to-day variability, including much higher transmittance values than observed at Tara. The main reason for this is the combination of both sea ice types (FYI and MYI), whereas the Tara floe consisted of only MYI. Consequently, the strong differences in optical properties of FYI and MYI, as parameterized here, strongly contribute to the overall energy budget. To overcome this problem, FYI/MYI fractions per grid cell (Kwok, 2004) could be used instead of the presented discrete distinction. However, such a data set is not yet available for the given time span.

Hudson et al. (2013) measured heat fluxes and calculated transmittance values of Arctic FYI in July/August 2012. However, a direct comparison of energy fluxes, as for the Tara measurements, is not possible, because the melt-pond concentration data set ends in December 2011. August transmittance in our study (0.087) is based on the observations

by Nicolaus et al. (2012), which is only half of the 0.16 found by Hudson et al. (2013). Hence, it may be assumed that heat fluxes through sea ice would be larger based on those measurements. Differences between both studies mainly result from differences in sea ice thickness during the respective campaigns as well as the different methods of quantifying transmittance (mean value vs. modal value) (Hudson et al., 2013).

4.3 Limitations

Measurements from Ice-Tethered Profilers (ITPs) (Krishfield et al., 2008) could be used as an alternative approach to estimate uncertainties of the new parameterization. They allow quantifying the heat content of the uppermost ocean and its changes. However, such a comparison would require a significant extension of the present study, integrating radiation fluxes to larger depths and through open water. Similarly, the inclusion of a radiation transfer model is beyond the aim of this study. The advantage of this study is the rather simplistic approach based on a seasonal parameterization of under-ice fluxes applied to existing large-scale data products.

An improvement of this study would be the inclusion of sea ice thickness (e.g. CryoSat-2, IceSat, OperationIceBridge) and snow depth (e.g. AMSR-E) observations from satellites. As with all other input data, the above mentioned products need to be consistent over many years and reliable during all seasons. But this is not the case yet, and even the most recent data sets have huge uncertainties or are not available after melt onset (e.g. Ricker et al. (2014)), which is the most important time with respect to transmitted heat fluxes. Hence these parameters are not applicable for such parameterizations yet. Instead, sea ice age is used as a proxy for ice thickness and snow depth distribution. It

570 also includes information about roughness and deformation of the sea ice surface. These
571 characteristics are crucial for the description of optical properties of sea ice.
572 In addition, including data sets of different model simulations, such as sea ice thickness,
573 snow depth, and melt pond fraction (e.g. Flocco et al., 2012;Schröder et al., 2014), can be
574 considered as an alternative approach for the presented calculations.
575
576 Another uncertainty in the presented heat flux calculations results from constant values
577 for the transmittance of melt ponds on FYI and MYI. Based on our existing data, it was
578 not possible to include a seasonality in melt pond transmittances, which represents the
579 different formation and evolution stages (Perovich and Polashenski, 2012). However,
580 the applied transmittances of melt ponds are modal values of a distribution function
581 (Nicolaus et al., 2012), representing a range of possible values. This has to be considered
582 when comparing our fluxes to other observations or model results. Over all, we expect
583 that the uncertainties resulting from the missing seasonal cycle have much smaller
584 impact than the timing of melt onset, which is discussed in the next section.
585
586 **4.4 Sensitivity studies**
587 Based on uncertainties of the independent input variables (timing and length of the melt
588 season, ice age, and melt pond fraction) several sensitivity studies have been performed
589 to estimate the uncertainty for the presented parameterization.
590 The first study studies the effect of altering the timing and duration of the melt season
591 on the solar heat input to the upper ocean. Three cases are discussed: shifting the melt
592 season dates by: (Case 1a) the average uncertainty of 4 days as given by (Markus et al.,
593 2009); (Case 1b) 7 days based on the temporal resolution of ice age data (once per
594 week) (Maslanik et al., 2011); and (Case 1c) (averaged) 14 days as derived from

595 comparisons with the Tara field data (Nicolaus et al., 2010a). Based on the observed
596 ongoing trend towards a lengthening of the melt season, all sensitivity studies were only
597 performed for earlier EMO and MO, and a later EFO and FO for the exemplary year 2011.
598 Extending the melt season by 4 days (Case 1a) results in Arctic-wide mean EMO on 12
599 May and MO on 27 May. This affects most regions primarily during periods of high sea
600 ice concentration and large surface solar irradiance. It results in an increase in total
601 annual solar heat input through sea ice to the ocean (Q_T) of 7% from 53.3×10^{19} J to
602 57.0×10^{19} J for the entire year 2011. The strongest increase of 20 % compared to the
603 reference melt onset dates was found in May, while the strongest absolute increase of
604 1.9×10^{19} J was found in June.
605
606 Including 7 days earlier (Case 1b) EMO (8 May) and MO (23 May) results in an
607 additional heat input of 5.9×10^{19} J (+11%) compared to the reference system for the
608 total annual heat input to the upper ocean. Shifting the melt season another 7 days (Case
609 1c) backwards (1 May and 16 May), the increase in Q_T is more than double compared to
610 the 7-day-shift (Tab. 3, 66.3×10^{19} J). The pronounced increase is most evident in May,
611 when 90% more light transmission was found than in the reference system. The
612 strongest absolute increase of 6.2×10^{19} J (transmittance from 0.054 to 0.067) was
613 calculated for June. The spatial distribution in the impact of the 14 days earlier EMO and
614 MO showed the largest increase of solar heat input to the upper ocean in the marginal
615 ice zone, with increases greater than 100% (Figure 7a).
616 Extending the melt season by 14 days (Case 1c) later EFO and FO (21 October and 2
617 November, respectively), results in a 1% increase of Q_T from 53.3×10^{19} J to 53.9×10^{19} J
618 (Fig. 7b). Since the surface solar radiation is much less than between April and June, the
619 change at the end of the melt season is small during August and September (increase of

9% from 7.02×10^{19} J to 7.65×10^{19} J). A 7 day or rather 4 day (Cases 1a and 1b) later EFO and FO have a negligible effect on the total annual transmitted heat flux of less than 1%.

In a second sensitivity study, the influence of the ice type was quantified. As the sea ice type data contain no uncertainty, the study is based on the ongoing trend towards a predominantly FYI-covered Arctic Ocean. The reference ice cover of 2011 consists of 56% FYI and 44% MYI in August 2011. Assuming that all sea ice in 2011 was MYI, the mean transmitted flux decreased by 34 % to 35.5×10^{19} J. In contrast, assuming that only FYI was present increased the mean transmitted flux by 18 % to 62.7×10^{19} J. Hence, the transition from a MYI to FYI dominated Arctic sea ice regime results in a further increase of solar heat flux under Arctic sea ice.

The third sensitivity study investigates the effects of melt pond fraction uncertainties. Here we consider two cases: (Case 3a) Rösel et al. (2012) give a mean uncertainty of 3% and (Case 3b) we estimate an uncertainty of 20% due to the neglected seasonal cycle. Adapting these assumptions, an increasing melt pond fraction of 3 % (20%) results in an increase of the transmitted heat flux of 1 % (9%).

Uncertainties in the solar surface radiation and sea ice concentration are not analyzed through additional sensitivity studies, because they impact the results linearly (Equation 2).

5 Summary and conclusions

The presented parameterization for light transmission through Arctic sea ice in combination with satellite-derived time series observations and re-analyses data

allowed the quantification of solar short-wave radiation fluxes through Arctic sea ice for the entire annual cycle over 33 years (1979 to 2011). The presented results suggest that 96% of the total annual solar heat input through sea ice occurs over only 4 months (May to August), with highest transmitted fluxes calculated for June. Over the time period 1979 to 2011, an increase in light transmission of 1.5%/year with regional maxima of 4.0% was found. Hence, the amount of short-wave radiation that may contribute to sea ice bottom melt has increased by 63% over this 33 year period. The results of our sensitivity studies show that energy fluxes strongly depend on the timing of melt onset, sea ice types (first and multi year ice), and melt pond fraction. These are the most critical parameters for the presented calculations and describe the most critical uncertainties. The calculated trends are affected by most of these uncertainties.

This study considers the fluxes through ice-covered ocean regions only. This highlights that changes in sea ice properties have a large impact on the sea ice and upper ocean energy budget, and that this impact adds to the obvious increase in energy input resulting from the observed decrease in ice covered area (open ocean effect). However, the ongoing retreat of sea ice will cause additional increases in radiation fluxes into the Arctic Ocean. The additional heat will also contribute to an increase of heat stored in the ocean mixed layer and will impact the melt season duration and timing, particularly during autumn freeze-up.

A comparison of trends in solar heat fluxes into the sea ice by Perovich et al. (2011a) with our calculated solar heat fluxes through sea ice both suggest similar increases in transmitted and absorbed energy. This additional energy input into the sea ice and the upper ocean would also impact inner sea ice structure as well as internal and basal melting. Studies from Perovich et al. (2011a) and Nicolaus et al. (2012) and (2013) reveal that fluxes through open water clearly dominate the transmitted heat flux signal,

and therefore, the effect of sea ice concentration becomes most obvious. Since our presented study focuses on changes in physical properties of sea ice and its effects, all calculated trends are corrected for the trend in sea ice concentration and fluxes through open water are neglected. Also, the effects of heat convection and advection, as well as lateral heat fluxes are not discussed due to the limited number of recent studies on that topic.

More investigations of bio-geo-physical interactions are needed to better quantify the effects of the changing physical environment on the ecosystem and element cycles, and vice versa. Additional work is also required to improve Arctic-wide snow depth and sea ice thickness data products. Those products should provide a good description of surface properties during the spring-summer-transition, when the largest uncertainties were found. Such time series might become available from new data products that merge observations from different satellites and sensor types (e.g. SMOS, CryoSat-2, AMSR-E), and potentially also numerical models. The non-existence of such reliable long-term and Arctic-wide data sets was the main motivation to develop the presented method, based on available parameters. Otherwise, the application of a radiation transfer model with adequate input (forcing) data would have been an obvious alternative.

Acknowledgements

We are most grateful to Jim Maslanik (University of Colorado Boulder), Thorsten Markus and Jeffrey Miller (both NASA Goddard Space Flight Center), Thomas Lavergne (OSISAF, Met Norway), and Anja Rösel and Larsch Kaleschke (both University of Hamburg) for data provision and support through manifold discussions on their data products and

processing details. We thank Christian Katlein (Alfred-Wegener-Institut Helmholtz-Zentrum für Polar- und Meeresforschung) and Martin Claussen (Max Planck Institute for Meteorology) for constructive comments on the manuscript, as well as Benjamin Lange (Alfred-Wegener-Institut Helmholtz-Zentrum für Polar- und Meeresforschung) for proofreading. We appreciate the efforts of the three anonymous reviewers and the scientific editor in improving the manuscript. The study was funded through the Remote Sensing Alliance of the Helmholtz Association and the Alfred-Wegener-Institut Helmholtz-Zentrum für Polar- und Meeresforschung.

ReferencesUncategorized References

Andersen, S., Breivik, L. A., Eastwood, S., Godøy, Ø., Lind, M., Porcires, M., and Schyberg, H.: OSI SAF Sea Ice Product Manual,v3. 5, EUMETSAT OSI SAF,Ocean and Sea Ice Sattelite Application Facility, Tech. Rep. SAF/OSI/met. no/TEC/MA/125, 2007.

Arrigo, K. R., Perovich, D. K., Pickart, R. S., Brown, Z. W., van Dijken, G. L., Lowry, K. E., Mills, M. M., Palmer, M. A., Balch, W. M., Bahr, F., Bates, N. R., Benitez-Nelson, C., Bowler, B., Brownlee, E., Ehn, J. K., Frey, K. E., Garley, R., Laney, S. R., Lubelczyk, L., Mathis, J., Matsuoka, A., Mitchell, B. G., Moore, G. W. K., Ortega-Retuerta, E., Pal, S., Polashenski, C. M., Reynolds, R. A., Schieber, B., Sosik, H. M., Stephens, M., and Swift, J. H.: Massive Phytoplankton Blooms Under Arctic Sea Ice, Science, 336, 1408-1408, Doi 10.1126/Science.1215065, 2012.

Barber, D. G., Fung, A. K., Grenfell, T. C., Nghiem, S. V., Onstott, R. G., Lytle, V. I., Perovich, D. K., and Gow, A. J.: The role of snow on microwave emission and scattering over first-year sea ice, Ieee Transactions on Geoscience and Remote Sensing, 36, 1750-1763, 10.1109/36.718643, 1998.

Comiso, J. C.: Large decadal decline of the Arctic multiyear ice cover, Journal of Climate, 25, 1176-1193, 2012.

Deal, C., Jin, M. B., Elliott, S., Hunke, E., Maltrud, M., and Jeffery, N.: Large-scale modeling of primary production and ice algal biomass within arctic sea ice in 1992, Journal of Geophysical Research-Oceans, 116, Artn C07004
Doi 10.1029/2010jc006409, 2011.

Dee, D. P., Uppala, S. M., Simmons, A. J., Berrisford, P., Poli, P., Kobayashi, S., Andrae, U., Balmaseda, M. A., Balsamo, G., and Bauer, P.: The ERA‐Interim reanalysis: Configuration and performance of the data assimilation system, Quarterly Journal of the Royal Meteorological Society, 137, 553-597, 2011.

729 Flocco, D., Schroeder, D., Feltham, D. L., and Hunke, E. C.: Impact of melt ponds on Arctic
730 sea ice simulations from 1990 to 2007, Journal of Geophysical Research-Oceans, 117,
731 Artn C09032
732 Doi 10.1029/2012jc008195, 2012.

733 Frey, K. E., Perovich, D. K., and Light, B.: The spatial distribution of solar radiation under
734 a melting Arctic sea ice cover, Geophysical Research Letters, 38, Artn L22501
735 Doi 10.1029/2011gl049421, 2011.

736 Grenfell, T. C., Light, B., and Perovich, D. K.: Spectral transmission and implications for
737 the partitioning of shortwave radiation in arctic sea ice, Annals of Glaciology, 44, 1-6,
738 2006.

739 Haas, C., Pfaffling, A., Hendricks, S., Rabenstein, L., Etienne, J. L., and Rigor, I.: Reduced ice
740 thickness in Arctic Transpolar Drift favors rapid ice retreat, Geophysical Research
741 Letters, 35, 10.1029/2008gl034457, 2008.

742 Hudson, S. R., Granskog, M. A., Sundfjord, A., Randelhoff, A., Renner, A. H. H., and Divine,
743 D. V.: Energy budget of first-year Arctic sea ice in advanced stages of melt, Geophysical
744 Research Letters, 40, 2679-2683, Doi 10.1002/Grl.50517, 2013.

745 Katlein, C., Nicolaus, M., and Petrich, C.: The anisotropic scattering coefficient of sea ice,
746 Journal of Geophysical Research-Oceans, 119, 842-855, Doi 10.1002/2013jc009502,
747 2014.

748 Krishfield, R., Toole, J., Proshutinsky, A., and Timmermans, M. L.: Automated Ice-
749 Tethered Profilers for Seawater Observations under Pack Ice in All Seasons, J Atmos
750 Ocean Tech, 25, 2091-2105, Doi 10.1175/2008jtecho587.1, 2008.

751 Kwok, R.: Annual cycles of multiyear sea ice coverage of the Arctic Ocean: 1999–2003,
752 Journal of Geophysical Research, 109, C11004, 10.1029/2003JC002238, 2004.

753 Lavergne, T., Killie, M. A., Eastwood, S., and Breivik, L.-A.: Extending the CryoClim Arctic
754 sea ice extent time series with operational OSI SAF products from 2008 onwards,
755 Norwegian Meteorological Institute note, 7, 2010.

756 Leu, E., Wiktor, J., Soreide, J. E., Berge, J., and Falk-Petersen, S.: Increased irradiance
757 reduces food quality of sea ice algae, Marine Ecology Progress Series, 411, 49-60, Doi
758 10.3354/Meps08647, 2010.

759 Light, B., Grenfell, T. C., and Perovich, D. K.: Transmission and absorption of solar
760 radiation by Arctic sea ice during the melt season, Journal of Geophysical Research:
761 Oceans (1978,Äì2012), 113, 2008.

762 Lindsay, R., Wensnahan, M., Schweiger, A., and Zhang, J.: Evaluation of Seven Different
763 Atmospheric Reanalysis Products in the Arctic*, Journal of Climate, 27, 2588-2606, Doi
764 10.1175/Jcli-D-13-00014.1, 2014.

765 Markus, T., Stroeve, J. C., and Miller, J. A.: Recent changes in Arctic sea ice melt onset,
766 freezeup, and melt season length, Journal of Geophysical Research, 114, C12024, Artn
767 C12024
768 Doi 10.1029/2009jc005436, 2009.

769 Maslanik, J., Stroeve, J., Fowler, C., and Emery, W.: Distribution and trends in Arctic sea
770 ice age through spring 2011, Geophysical Research Letters, 38, Artn L13502
771 Doi 10.1029/2011gl047735, 2011.

772 Maslanik, J. A., Fowler, C., Stroeve, J., Drobot, S., Zwally, J., Yi, D., and Emery, W.: A
773 younger, thinner Arctic ice cover: Increased potential for rapid, extensive sea-ice loss,
774 Geophysical Research Letters, 34, Artn L24501
775 Doi 10.1029/2007gl032043, 2007.

776 Mundy, C. J., Barber, D. G., and Michel, C.: Variability of snow and ice thermal, physical
777 and optical properties pertinent to sea ice algae biomass during spring, J Marine Syst, 58,
778 107-120, Doi 10.1016/J.Jmarsys.2005.07.003, 2005.

779 Mundy, C. J., Ehn, J. K., Barber, D. G., and Michel, C.: Influence of snow cover and algae on
780 the spectral dependence of transmitted irradiance through Arctic landfast first-year sea
781 ice, Journal of Geophysical Research-Oceans, 112, Artn C03007
782 Doi 10.1029/2006jc003683, 2007.

783 Nicolaus, M., Haas, C., Bareiss, J., and Willmes, S.: A model study of differences of snow
784 thinning on Arctic and Antarctic first-year sea ice during spring and summer, Annals of
785 Glaciology, 44, 147-153, 2006.

786 Nicolaus, M., Gerland, S., Hudson, S. R., Hanson, S., Haapala, J., and Perovich, D. K.:
787 Seasonality of spectral albedo and transmittance as observed in the Arctic Transpolar
788 Drift in 2007, Journal of Geophysical Research-Oceans, 115, Artn C11011
789 Doi 10.1029/2009jc006074, 2010a.

790 Nicolaus, M., Hudson, S. R., Gerland, S., and Munderloh, K.: A modern concept for
791 autonomous and continuous measurements of spectral albedo and transmittance of sea
792 ice, Cold Regions Science and Technology, 62, 14-28, 2010b.

793 Nicolaus, M., Katlein, C., Maslanik, J., and Hendricks, S.: Changes in Arctic sea ice result in
794 increasing light transmittance and absorption, Geophysical Research Letters, 39,
795 submitted, Artn L24501
796 Doi 10.1029/2012gl053738, 2012.

797 Nicolaus, M., Arndt, S., Katlein, C., Maslanik, J., and Hendricks, S.: Correction to "Changes
798 in Arctic sea ice result in increasing light transmittance and absorption", Geophysical
799 Research Letters, 40, 2699-2700, 10.1002/grl.50523, 2013.

800 Perovich, D. K.: The Optical Properties of Sea Ice, U.S. Cold Reg. Res. and Eng. Lab.
801 Monogr., Hannover, 25 pp, 1996.

802 Perovich, D. K., Roesler, C. S., and Pegau, W. S.: Variability in Arctic sea ice optical
803 properties, Journal of Geophysical Research-Oceans, 103, 1193-1208,
804 10.1029/97jc01614, 1998.

805 Perovich, D. K., Grenfell, T. C., Light, B., and Hobbs, P. V.: Seasonal evolution of the albedo
806 of multiyear Arctic sea ice, Journal of Geophysical Research-Oceans, 107, Artn 8044
807 Doi 10.1029/2000jc000438, 2002.

808 Perovich, D. K.: On the aggregate-scale partitioning of solar radiation in Arctic sea ice
809 during the Surface Heat Budget of the Arctic Ocean (SHEBA) field experiment, Journal of
810 Geophysical Research-Oceans, 110, Artn C03002
811 Doi 10.1029/2004jc002512, 2005.

812 Perovich, D. K., Light, B., Eicken, H., Jones, K. F., Runciman, K., and Nghiem, S. V.:
813 Increasing solar heating of the Arctic Ocean and adjacent seas, 1979–2005: Attribution
814 and role in the ice‐albedo feedback, Geophysical Research Letters, 34, 2007a.

815 Perovich, D. K., Nghiem, S. V., Markus, T., and Schweiger, A.: Seasonal evolution and
816 interannual variability of the local solar energy absorbed by the Arctic sea ice-ocean
817 system, Journal of Geophysical Research-Oceans, 112, Artn C03005
818 Doi 10.1029/2006jc003558, 2007b.

819 Perovich, D. K., and Richter-Menge, J. A.: Loss of Sea Ice in the Arctic*, Annual Review of
820 Marine Science, 1, 417-441, 2009.

821 Perovich, D. K., Jones, K. F., Light, B., Eicken, H., Markus, T., Stroeve, J., and Lindsay, R.:
822 Solar partitioning in a changing Arctic sea-ice cover, Annals of Glaciology, 52, 192-196,
823 2011a.

824 Perovich, D. K., Richter-Menge, J. A., Jones, K. F., Light, B., Elder, B. C., Polashenski, C.,
825 Laroche, D., Markus, T., and Lindsay, R.: Arctic sea-ice melt in 2008 and the role of solar
826 heating, Annals of Glaciology, 52, 355-359, 2011b.

827 Perovich, D. K., and Polashenski, C.: Albedo evolution of seasonal Arctic sea ice,
828 Geophysical Research Letters, 39, Artn L08501
829 Doi 10.1029/2012gl051432, 2012.

830 Popova, E. E., Yool, A., Coward, A. C., Dupont, F., Deal, C., Elliott, S., Hunke, E., Jin, M. B.,
831 Steele, M., and Zhang, J. L.: What controls primary production in the Arctic Ocean?
832 Results from an intercomparison of five general circulation models with
833 biogeochemistry, Journal of Geophysical Research-Oceans, 117, Artn C00d12
834 Doi 10.1029/2011jc007112, 2012.

835 Ricker, R., Hendricks, S., Helm, V., Skourup, H., and Davidson, M.: Sensitivity of CryoSat-2
836 Arctic sea-ice freeboard and thickness on radar-waveform interpretation, The
837 Cryosphere, 8, 1607-1622, 2014.

838 Rösel, A., and Kaleschke, L.: Exceptional melt pond occurrence in the years 2007 and
839 2011 on the Arctic sea ice revealed from MODIS satellite data, Journal of Geophysical
840 Research-Oceans, 117, 10.1029/2011jc007869, 2012.

841 Rösel, A., Kaleschke, L., and Birnbaum, G.: Melt ponds on Arctic sea ice determined from
842 MODIS satellite data using an artificial neural network, Cryosphere, 6, 431-446,
843 10.5194/tc-6-431-2012, 2012.

844 Schröder, D., Feltham, D. L., Flocco, D., and Tsamados, M.: September Arctic sea-ice
845 minimum predicted by spring melt-pond fraction, Nature Climate Change, 2014.

846 Stroeve, J. C., Markus, T., Boisvert, L., Miller, J., and Barrett, A.: Changes in Arctic melt
847 season and implications for sea ice loss, Geophysical Research Letters, 41, 1216-1225,
848 Doi 10.1002/2013gl058951, 2014.

849 Wang, C., Granskog, M. A., Gerland, S., Hudson, S. R., Perovich, D. K., Nicolaus, M., Ivan
850 Karlsen, T., Fossan, K., and Bratrein, M.: Autonomous observations of solar energy
851 partitioning in first‐year sea ice in the Arctic Basin, Journal of Geophysical Research:
852 Oceans, 119, 2066-2080, 2014.

853 Wassmann, P., and Reigstad, M.: Future Arctic Ocean seasonal ice zones and implications
854 for pelagic-benthic coupling, 2011.
855

Figure 1: Classification of sea ice (a) types and (b) surface properties as used in this study. The timing of each phase results from the status of the sea ice. Depending on the season, different sea ice types co-exist. Abbreviations: FYI: first year ice, MYI: multi year ice, EMO: early melt onset, MO: melt onset, EFO: early freeze onset, FO: freeze onset.

Figure 2: (a) Total transmittance of sea ice during each phase (Fig. 1). In this figure, melt pond concentrations of 26 % are assumed for first year ice (FYI) and 29 % are assumed for multi year ice (MYI). (b) Transmittance of bare ice during each phase (see Figure 1). Transmittance values for single ice classes are given in Table 1. The illustrated evolution of transmittance values is based on analyses from previous field campaigns and observations. Abbreviations: see Figure 1.

Figure 3: Monthly mean of total solar heat input ($Q_T(x,y)$) under Arctic sea ice (ice covered areas only) for the year 2011.

Figure 4: Annual total solar heat input ($Q_T(x,y)$) through Arctic sea ice. (a) Average and (b) trend from 1979 to 2011. The trend is normalized for the trend in sea ice concentration. Purple shaded areas were not covered with sea ice during the maximum extent in all years.

Figure 5: Arctic-wide total solar heat flux under sea ice (Q_T) (black) and monthly Arctic-wide solar heat input for May to August (colored) and its trend from 1979 to 2011. The data are corrected for the trend in sea ice concentration. Areas that were not ice covered at any time in 2011 or during a certain month in 2011 are excluded from the analyses.

Figure 6: (a) Transmitted total solar heat input and (b) total transmittance during the drift of Tara in 2007 (*Nicolaus et al.,* 2010b). Compared are in situ measurements (green) with the presented method (red) and the presented method, but using the observed dates for phase transitions. Between 16 July and 14 August (dotted lines) a comparison is not reasonable since the sensor was strongly influenced by biological processes during Tara.

Figure 7: Changes in annual total solar heat input ($Q_T(x,y)$) through sea ice in 2011, resulting from a sensitivity study assuming an extended melt season. (a) 14 days earlier early melt onset and melt onset and (b) 14 days later early freeze onset and freeze onset than in the reference method, based on *Markus et al.* (2007).

Table 1: Data sources of the different parameters used in this study.

Parameter	Time period	Source
Sea ice concentration	1979 – 2007 2008 – 2011	OSI SAF, reprocessed data OSI SAF, operated data (*Andersen et al.*, 2007)
Sea ice age	1979 – 2011	(*Maslanik et al.*, 2007;2011)
Downward surface solar radiation	1979 – 2011	ECMWF (*Dee et al.*, 2011)
Melt and freeze onset	1979 – 2005 2006 – 2010 2011	SSMR AMSR-E SSM/IS (*Markus et al.*, 2011)
Melt pond fraction	1979 – 1999 2000 – 2011	Constant fraction as in 2011 ICDC (*Rösel et al.*, 2012)

Table 2: Transmittance values of different sea ice and surface types. Abbreviations: FYI: first year ice, MYI: multi year ice, Phase I: winter, MO: melt onset, Phase IV: summer, FO: freeze onset, Threshold: transition from open ocean to sea ice and vice versa.

	Phase I (winter)	At MO	Phase IV (summer)	At FO	Threshold
FYI, pond covered sea ice	0.002	0.04	0.087	0.04	0.4
MYI, pond covered sea ice	0.002	0.02	0.05	0.02	0.4
FYI, bare ice/snow	0.001	0.017	0.04	0.017	0.17
FYI, melt ponds	0.22				
MYI, bare ice/snow	0.0	0.004	0.01	0.004	0.07
MYI, melt ponds	0.15				
Open ocean	0.93				

Table 3: Annual Arctic-wide solar heat input (and relative changes) under sea ice (Q_T) in 2011 for the reference method and sensitivity study 1: Changes in melt season duration by a shift of 4 days (data uncertainty, *Markus et al. (2009)*), 7 days (estimated uncertainty due to only weekly sea ice age data by *Maslanik et al. (2009)*), and 14 days (derived from comparisons to field data, *Nicolaus et al. (2010a)*). All trends were only performed towards a prolongation of the melt season. All numbers are in 10^{19} J.

	Reference system	Changing EMO and MO			Changing EFO and FO		
		- 4 days	- 7 days	- 14 days	- 4 days	- 7 days	- 14 days
Apr	1.00	1.17 (+17%)	1.19 (+19%)	1.45 (+45%)	1.00 (0%)	1.00 (0%)	1.00 (0%)
May	5.53	6.64 (+20%)	7.35 (+33%)	10.5 (+90%)	5.53 (0%)	5.53 (0%)	5.53 (0%)
June	20.9	22.8 (+9%)	24.0 (+15%)	27.1 (+30%)	20.9 (0%)	20.9 (0%)	20.9 (0%)
Jul	18.4	18.7 (+2%)	19.1 (+4%)	19.7 (+7%)	18.4 (0%)	18.4 (0%)	18.4 (0%)
Aug	6.33	6.34 (0%)	6.42 (+1%)	6.48 (+2%)	6.46 (+2%)	6.51 (+3%)	6.68 (+5%)
Sep	0.69	0.69 (0%)	0.69 (0%)	0.69 (0%)	0.74 (+7%)	0.81 (17%)	0.97 (+41%)
Jan-Dec	53.3	57.0 (+7%)	59.2 (+11%)	66.3 (+24%)	53.4 (0%)	53.6 (+0%)	53.9 (+1%)

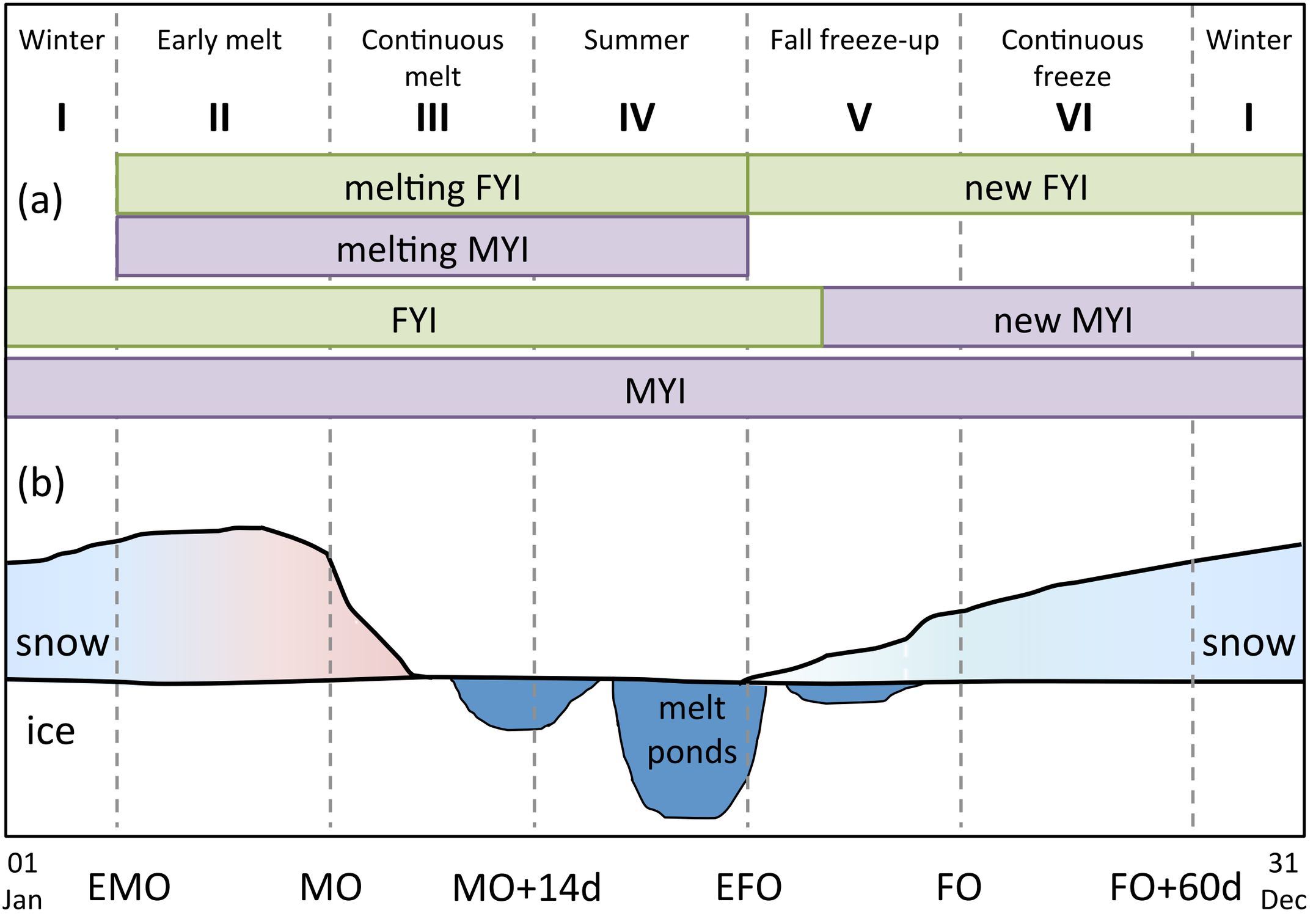
Winter
Early melt
Continuous melt
Summer
Fall freeze-up
Continuous freeze
Winter
I
II
III
IV
V
VI
I
(a)
melting FYI
new FYI
melting MYI
FYI
new MYI
MYI
(b)
snow
snow
ice
melt ponds
01 Jan
EMO
MO
MO+14d
EFO
FO
FO+60d
31 Dec

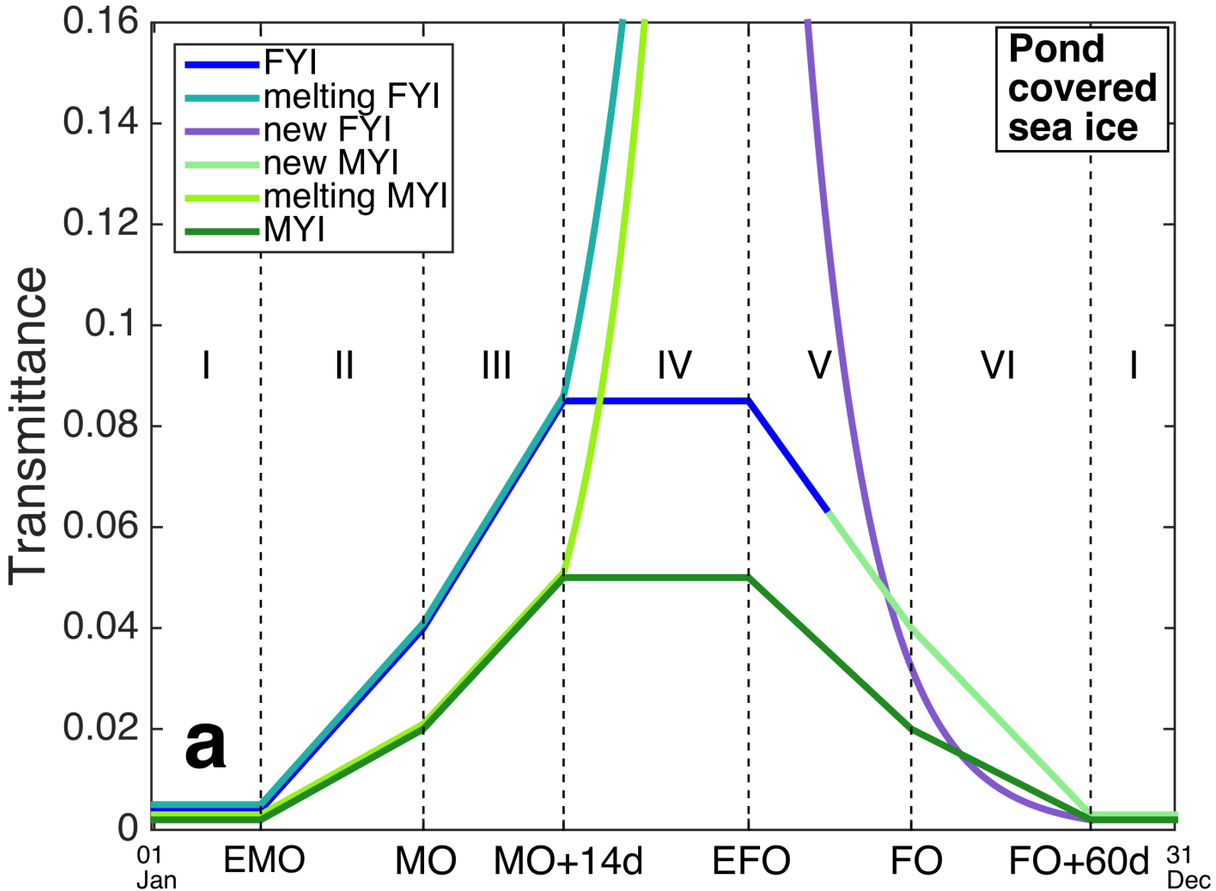
Pond covered sea ice
FYI
melting FYI
new FYI
new MYI
melting MYI
MYI
Transmittance
0.16
0.14
0.12
0.1
0.08
0.06
0.04
0.02
0
I
II
III
IV
V
VI
I
a
01 Jan
EMO
MO
MO+14d
EFO
FO
FO+60d
31 Dec

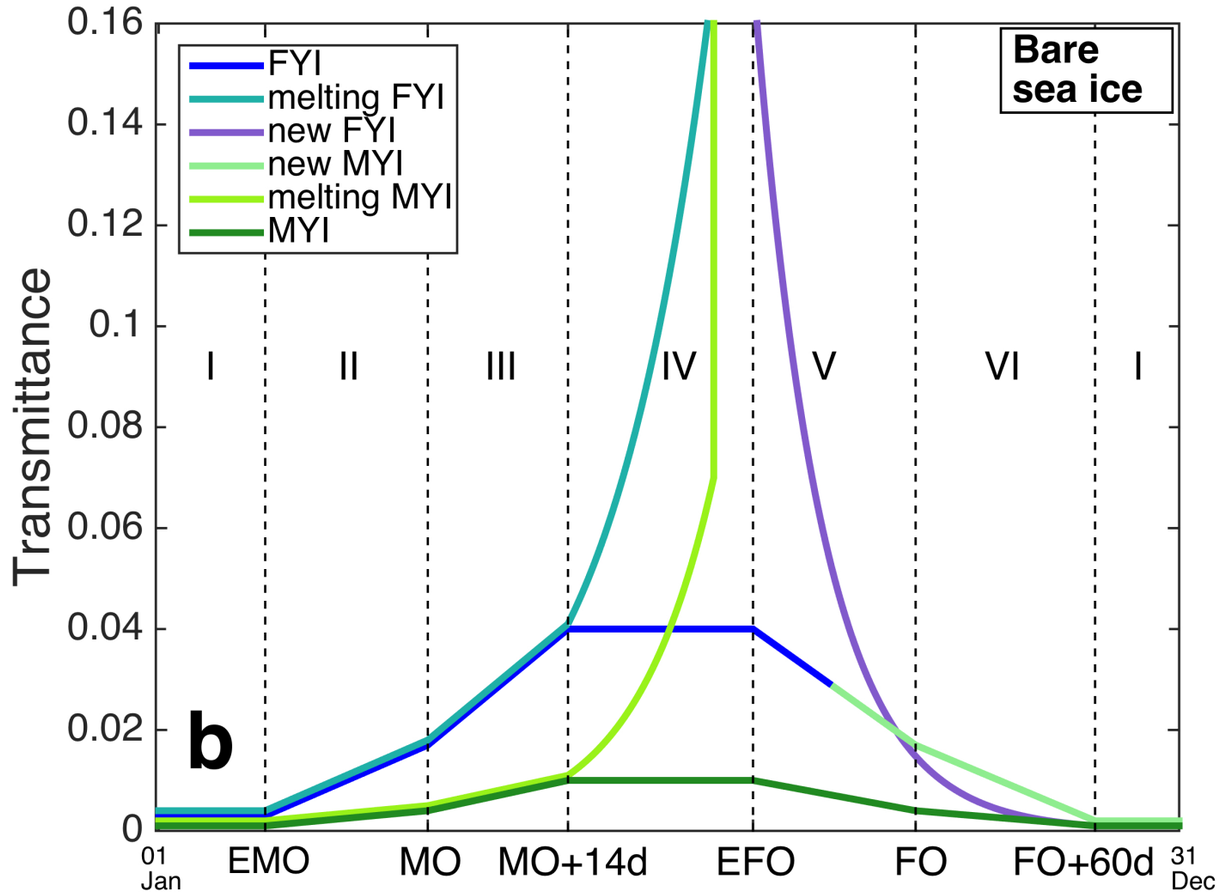
Bare sea ice
FYI
melting FYI
new FYI
new MYI
melting MYI
MYI
Transmittance
0.16
0.14
0.12
0.1
0.08
0.06
0.04
0.02
0
I
II
III
IV
V
VI
I
b
01 Jan
EMO
MO
MO+14d
EFO
FO
FO+60d
31 Dec

Apr

May

Jun

Jul

Aug

Sep

180°W
70°N
75°N
80°N
85°N
120°W
120°E
60°W
60°E
0°

Solar heat input [10^5 J m^{-2}]
20
18
16
14
12
10
8
6
4
2
0

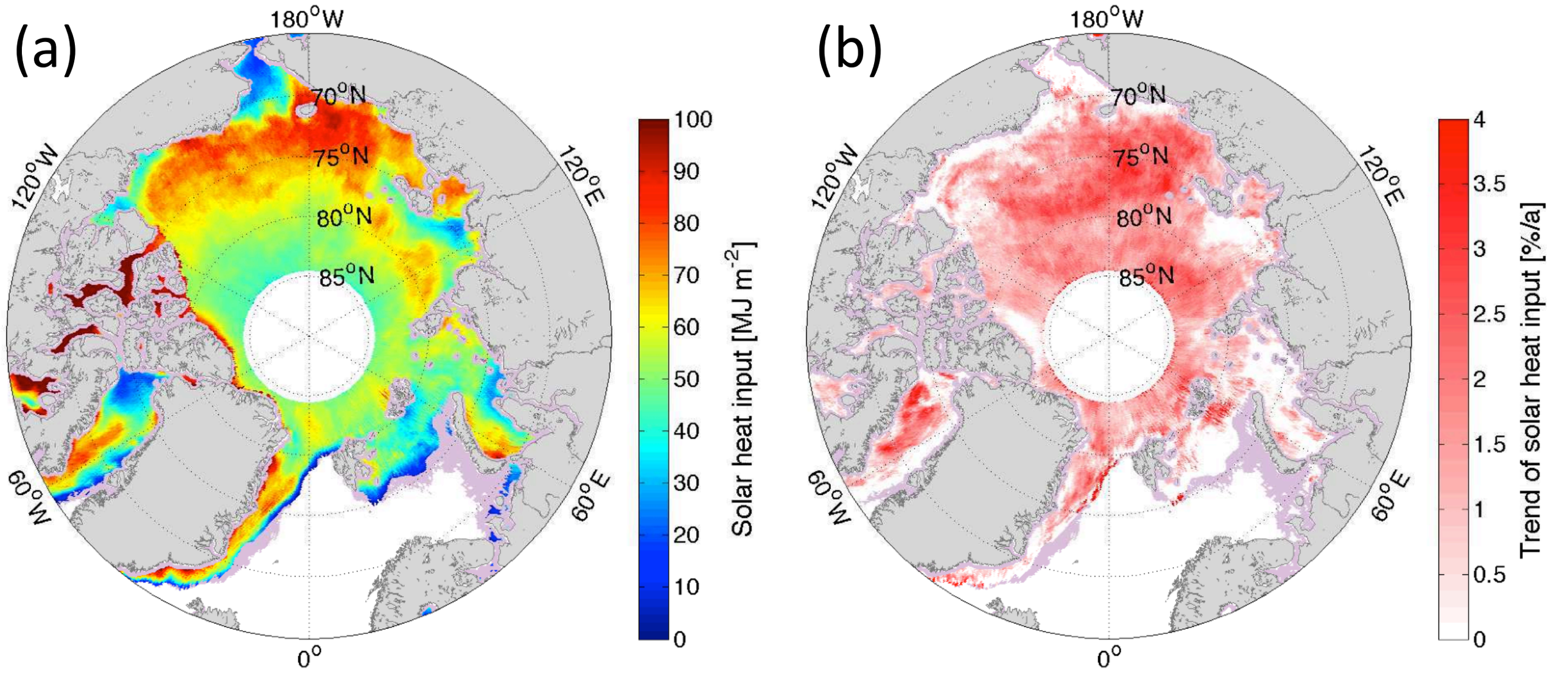
(a)
180°W
70°N
75°N
80°N
85°N
120°W
120°E
60°W
60°E
0°
100
90
80
70
60
50
40
30
20
10
0
Solar heat input [MJ m-2]
(b)
180°W
70°N
75°N
80°N
85°N
120°W
120°E
60°W
60°E
0°
4
3.5
3
2.5
2
1.5
1
0.5
0
Trend of solar heat input [%/a]

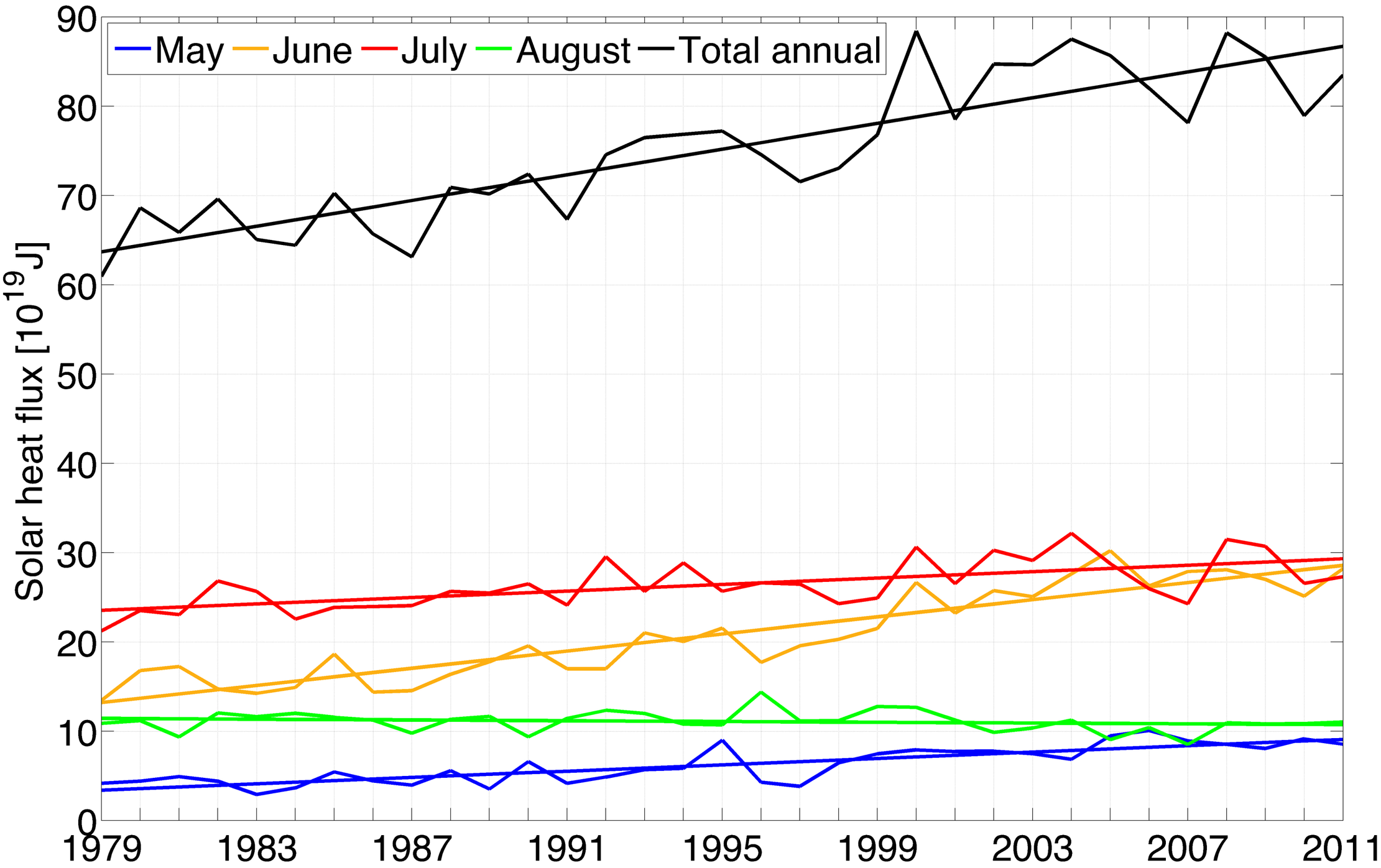
May
June
July
August
Total annual
Solar heat flux [10^19 J]
90
80
70
60
50
40
30
20
10
0
1979
1983
1987
1991
1995
1999
2003
2007
2011

Parameterization (Markus et al., 2009; melt onset)
In-situ measurements during Tara
Parameterization with observed melt onset (Tara)

Solar heat input [Wm^{-2}]

0
5
10
15
20
25

a

Transmittance

0
0.02
0.04
0.06
0.08
0.1
0.12

b

01-May
15-May
01-Jun
15-Jun
01-Jul
15-Jul
01-Aug
15-Aug
01-Sep
15-Sep

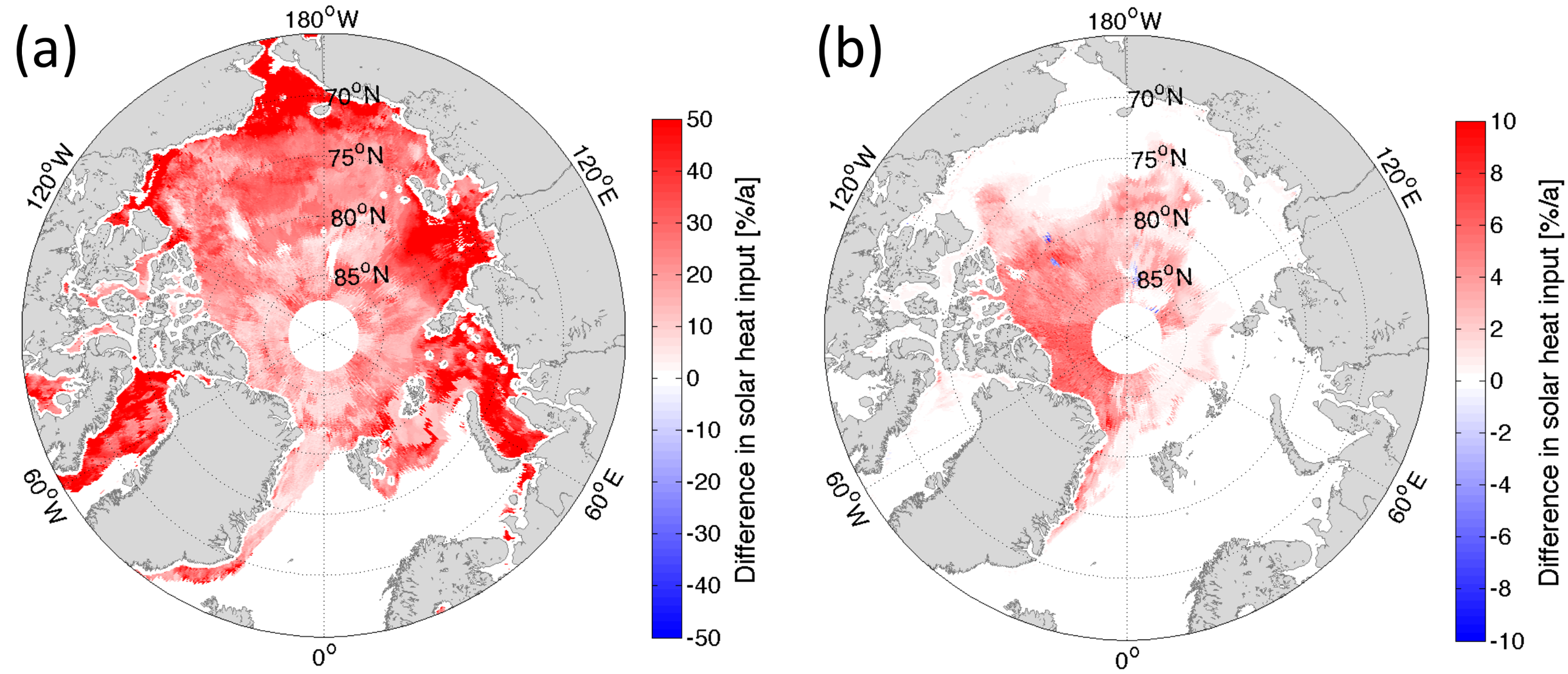
(a)
180°W
70°N
75°N
80°N
85°N
120°W
120°E
60°W
60°E
0°
50
40
30
20
10
0
-10
-20
-30
-40
-50
Difference in solar heat input [%/a]
(b)
180°W
70°N
75°N
80°N
85°N
120°W
120°E
60°W
60°E
0°
10
8
6
4
2
0
-2
-4
-6
-8
-10
Difference in solar heat input [%/a]